Research Article

Contralateral S1 function is involved in electroacupuncture treatment-mediated recovery after focal unilateral M1 infarction

https://doi.org/10.4103/1673-5374.327355

Date of submission: March 4, 2021

Date of decision: May 18, 2021

Date of acceptance: July 11, 2021

Date of web publication: November 12, 2021

Lu-Lu Yao[1], Si Yuan[1], Zhen-Nan Wu[1], Jian-Yu Luo[1], Xiao-Rong Tang[1], Chun-Zhi Tang[1], Shuai Cui[1, 2, *], Neng-Gui Xu[1, *]

From the Contents

Graphical Abstract *Neuronal activity in the contralateral S1 underlies the mechanism of how electroacupuncture (EA) treatment at GV20 and GV14 mediates recovery after unilateral M1 infarction*

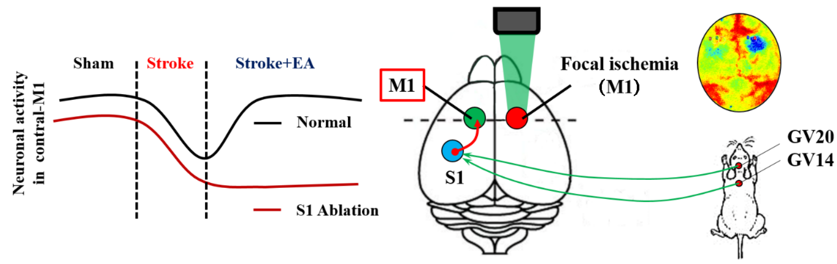

Abstract

Acupuncture at acupoints *Baihui* (GV20) and *Dazhui* (GV14) has been shown to promote functional recovery after stroke. However, the contribution of the contralateral primary sensory cortex (S1) to recovery remains unclear. In this study, unilateral local ischemic infarction of the primary motor cortex (M1) was induced by photothrombosis in a mouse model. Electroacupuncture (EA) was subsequently performed at acupoints GV20 and GV14 and neuronal activity and functional connectivity of contralateral S1 and M1 were detected using *in vivo* and *in vitro* electrophysiological recording techniques. Our results showed that blood perfusion and neuronal interaction between contralateral M1 and S1 is impaired after unilateral M1 infarction. Intrinsic neuronal excitability and activity were also disturbed, which was rescued by EA. Furthermore, the effectiveness of EA treatment was inhibited after virus-mediated neuronal ablation of the contralateral S1. We conclude that neuronal activity of the contralateral S1 is important for EA-mediated recovery after focal M1 infarction. Our study provides insight into how the S1–M1 circuit might be involved in the mechanism of EA treatment of unilateral cerebral infarction. The animal experiments were approved by the Committee for Care and Use of Research Animals of Guangzhou University of Chinese Medicine (approval No. 20200407009) April 7, 2020.

Key Words: brain plasticity; electroacupuncture; electrophysiology recording; neuronal activity; primary motor cortex; primary sensory cortex; stroke

Chinese Library Classification No. R459.9; R364; R741

Introduction

Motor deficit is a common consequence of stroke that seriously affects patient quality of life (Hatem et al., 2016). Therefore, developing effective rehabilitative interventions to promote functional recovery after stroke has attracted considerable attention from researchers (Murphy and Corbett, 2009; Cramer, 2018). Acupuncture treatment for stroke has been practiced in China for over 2000 years and has been recommended by the World Health Organization (WHO) as an alternative and complementary strategy (Chavez et al., 2017) . In recent decades, acupuncture has been demonstrated to improve function after stroke in the clinical neurorehabilitation setting (Wu et al., 2010). Although preclinical studies have shown potential mechanisms underlying acupuncture treatment in patients undergoing stroke rehabilitation, they have not been fully elucidated (Wang et al., 2014; Lu et al., 2016). *Baihui* (GV20) and *Dazhui* (GV14) are acupoints commonly used for stroke treatment that are both located on the “Du meridian,” which interacts with the brain (Wang et al., 2014; Chang et al., 2018). A large number of animal experiments have shown that acupuncture at GV20 and GV14 can reduce excitotoxicity, enhance neurogenesis, and

[1]South China Research Center for Acupuncture and Moxibustion, Medical College of Acupuncture Moxibustion and Rehabilitation, Guangzhou University of Chinese Medicine, Guangzhou, Guangdong Province, China; [2]Research Institute of Acupuncture and Meridian, Anhui University of Chinese Medicine, Hefei, Anhui Province, China

***Correspondence to:** Neng-Gui Xu, PhD, ngxu8018@gzucm.edu.cn; Shuai Cui, PhD, cuishuai@gzucm.edu.cn.
https://orcid.org//0000-0002-7945-9177 (Neng-Gui Xu); http://orcid.org/0000-0003-1457-6759 (Shuai Cui)

***Funding:** This work was supported by Guangzhou University of Chinese Medicine and by grants from General Program of the National Natural Science Foundation of China (No. 81774406, to NGX), Youth Program of the National Natural Science Foundation of China (No. 82004469, to LLY), Fellowship of China postdoctoral Science Foundation (No. 2020M672601, to LLY), Opening Operation Program of Key Laboratory of Acupuncture and Moxibustion of Traditional Chinese Medicine in Guangdong (No. 2017B030314143, to NGX).*

***How to cite this article:** Yao LL, Yuan S, Wu ZN, Luo JY, Tang XR, Tang CZ, Cui S, Xu NG (2022) Contralateral S1 function is involved in electroacupuncture treatment-mediated recovery after focal unilateral M1 infarction. Neural Regen Res 17(6):1310-1317.*

promote the release of neurotrophic factors in the brain (e.g., brain-derived neurotrophic factor, nuclear factor kappa B, tropomyosin-related kinase B), which reduces cerebral infarct volume and improves sensorimotor function (Cheng et al., 2014; Kim et al., 2014; Wang et al., 2014; Chang et al., 2018; Park et al., 2019). However, whether the neuroprotective effects of electroacupuncture (EA) treatment in focal ischemic stroke result from effects on neuronal activity or network connectivity beyond the molecular level remains unknown.

A considerable body of literature has demonstrated that neuroplasticity processes occur in the brain after stroke (Murphy and Corbett, 2009; Johansson, 2011). Not only do brain regions near the infarction reorganize, but remote regions as well (Dancause and Nudo, 2011). During functional recovery, decreased activation of the ipsilateral infarcted brain region can induce activation of the contralateral cortex (Cramer and Crafton, 2006; Cramer, 2008). Clinical trials using functional magnetic resonance imaging (fMRI) and positron emission tomography (PET) have shown that the cerebral cortex contralateral to the infarction plays an important role in recovery of function (Calautti and Baron, 2003; Buetefisch, 2015). In particular, unilateral infarction of the somatosensory or motor cortex leads to structural and functional changes in the corresponding cortex of the intact contralateral hemisphere (Reinecke et al., 2003; Gonzalez et al., 2004). Takatsuru et al. (2009) reported that the contralateral somatosensory cortex can compensate for the loss of ipsilateral somatosensory cortex by enhancing neuronal activity and increasing the expression of stable spines, thereby establishing new sensory processing. However, the role of the contralateral primary sensory cortex (S1) in EA-mediated recovery after primary motor cortex (M1) infarction remains elusive.

Previous studies have revealed the importance of S1 in motor function (Pavlides et al., 1993; Vidoni et al., 2010; Mathis et al., 2017) and have shown that M1 receives strong input from S1 (Petrof et al., 2015; Kinnischtzke et al., 2016). Accumulating evidence indicates that somatosensory function impairment may be a major contributor to motor dysfunction in several disorders, including stroke, dystonia, and ataxia (Hiraba et al., 2000). Sensory processing and movement production are closely connected from a functional perspective (Borich et al., 2015; Bolognini et al., 2016). In somatosensory stroke patients, the sensation induced by EA is highly related to the motor cortex and could be a predictor for stroke recovery (Bai et al., 2013). In addition, EA stimulation can enhance somatosensory evoked potentials in animal models of stroke (Si et al., 1998). Furthermore, EA treatment can increase functional connectivity between the ipsilateral motor cortex and sensory cortex (Li et al., 2021). In contrast to these studies, which focused on the infarcted hemisphere after focal ischemia, our study aimed to uncover the function of contralateral S1. Based on the known structural and functional interactions between S1 and M1 as reported above, and previous studies which have suggested an important role of the contralateral cortex in cerebral infarction (Murase et al., 2004; Takatsuru et al., 2009), we hypothesized that contralateral neuronal activity in S1 plays a key role in functional recovery after M1 infarction.

This study used *in vivo* and *in vitro* electrophysiological recording to examine neuronal activity in both S1 and M1 contralateral to the infarction and explore how the interaction between the two brain regions is involved in the effects of EA at GV20 and GV14 for the treatment of photothrombosis-induced focal stroke.

Materials and Methods

Animals

C57BL/6J mice were purchased from the Animal Laboratory Center of Guangzhou University of Chinese Medicine (license No. SCXK (Yue) 2018-0034). One hundred and fifty male mice weighing 25–35 g and aged 7–12 weeks were used for this study. The mice were housed in cages (5 mice/cage) with an ambient temperature of 25 ± 2°C, a 12-hour light-dark cycle, and *ad libitum* access to water and food. Animal care and experimental manipulation were conducted in accordance with the National Institutes of Health Guide for the Care and Use of Laboratory Animals and approved by the Committee for Care and Use of Research Animals of Guangzhou University of Chinese Medicine (approval No. 20200407009) April 7, 2020). This study is reported in accordance with the Animal Research: Reporting of *In Vivo* Experiments guidelines 2.0.

Mice were allocated randomly to the following three groups with 50 mice in each group using the random number table method: stroke (photochemical stroke model), stroke + EA (photochemical stroke plus EA treatment), and sham.

Photochemical modeling

A focal ischemic stroke was induced at M1FL using the photothrombosis technique as previously described (Takatsuru et al., 2009; Cui et al., 2020; Yao et al., 2020). Briefly, 100 male mice were anesthetized with an intraperitoneal injection of 1.25% avertin solution (80 mg/kg; Sigma-Aldrich, St. Louis, MO, USA). Approximately 10 minutes before surgery, 1.5% Rose Bengal solution (10 µL/g, Sigma-Aldrich), which can induce infarction after laser irradiation, was injected intraperitoneally. The targeted brain region was located in the right M1FL (forelimb region of M1) (coordinates: anterior-posterior (AP), +0.74 mm; medial-lateral (M/L), +1.5 mm) from the superficial) (Paxinos and Franklin, 2013). Irradiation wave length and power were 530 nm and 15mW, respectively, as described previously (Cui et al., 2020; Yao et al., 2020). After 10 minutes of irradiation, the infarcted area was examined using a laser speckle imaging system (PeriCam PSI; Perimed, Stockholm, Sweden).

Laser speckle blood flow imaging

To evaluate successful establishment of the ischemic model (greater than 30% decrease in blood perfusion in the infarcted site compared to the healthy site), blood perfusion was measured in all experimental groups using the laser speckle blood flow imaging system within 24 hours of each manipulation. Briefly, the mice were anesthetized with 2% isoflurane (Sigma-Aldrich) and fixed on a stereotaxic apparatus (RWD Biotechnology Co., Ltd., Shenzhen, Guangdong Province, China). After exposing the skull, the target brain area was imaged using the laser for a 5-minute recording. Total brain blood flow was recorded in a 60 mm^2 target area. The target areas were recorded in the ipsilateral M1FL (forelimb region of M1), ipsilateral S1FL (forelimb region of S1), contralateral M1FL (forelimb region of M1), and contralateral S1FL (forelimb region of S1) were approximately 0.78 mm^2.

EA treatment

Thirty-eight mice were treated with EA within 2 hours of stroke induction and for analysis. The mice were anesthetized with isoflurane and then placed in the prone position. Following routine sterilization of the scalp and neck, a disposable aseptic acupuncture needle (ϕ 0.18 × 10 mm) was inserted at GV20 (located at the midpoint of the line connecting the tip of the mouse ear) with needle angle 15° to a depth of 2 to 3 mm and GV14 (located at the depression under the spinous process of the seventh cervical vertebra) with needle angle 45° to a depth of 2 to 3 mm (**Figure 1**) (Wang et al., 2014; Chang et al., 2018). EA stimulus was delivered for 15 minutes using the HANS EA apparatus (HANS-200A/100B, HANS, China) with the following parameters: sparse wave, 2 Hz; dense wave, 10 Hz; and current, 1 mA. The mice showed visible muscle contraction near the acupoint during stimulus (Xing et al., 2018).

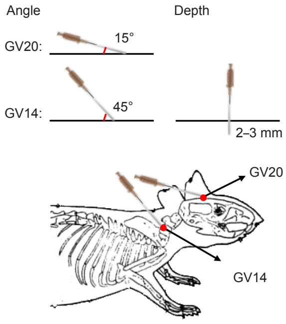

Figure 1 | Schematic diagram of needle insertion technique and location of acupoints.
GV14: *Dazhui*; GV20: *Baihui*.

Electrophysiological recording *in vivo* using multi-channel recording technique
The day after modeling, mice were maintained with 1% isoflurane and fixed on the stereotaxic apparatus. The skull was exposed after sterilization. Electrodes were then inserted into the contralateral M1 (primary motor cortex in the right hemisphere) (A/P: +0.74 mm, M/L: –1.5 mm, dorsal-ventral (D/V): 0.8–1.10 mm, Layer 5/6) and contralateral S1 (somatosensory cortex in the right hemisphere) (A/P: +0.02 mm, M/L: –2.04 mm, D/V: 0.8–1.10 mm, Layer 5/6) (Paxinos and Franklin, 2013; Sachidhanandam et al., 2013; Mathis et al., 2017; Liang et al., 2019; Vecchia et al., 2020). Eight matrix electrodes were used to record spontaneous discharges of S1FL and M1FL using a multichannel recording system (Plexon Inc., Dallas, TX, USA). Spikes and local field potential (LFP) were recorded for 5 minutes in each group. For coherence testing, two separate electrodes were simultaneously inserted into the two brain regions to record neuronal activity. An offline sorter (Plexon Inc.) was used to filter the signal and processed signals were analyzed using NeuroExplorer (Nex Technologies, Lexington, MA, USA). Units were categorized as neuronal cluster with similar firing properties.

The activity of interneurons (inhibitory neurons) and pyramidal cells (excitatory neurons) detected during electrophysiological recording *in vivo* was distinguished based on firing rate and waveform characteristics as follows (Csicsvari et al., 1999; Bartho et al., 2004): (1) Mean of auto correlogram: pyramidal cells show an advantage at short peak-peak spacing (3–10 ms) and exponentially decay after exhibiting a characteristic 3–5 ms peak spacing, while interneurons show a longer spike latency and slower decay. (2) Spike asymmetry: in pyramidal cells, the peak value before the valley point is larger than the peak value after the valley point, while in interneurons, the peak value after the valley point is larger (Csicsvari et al., 1998). (3) Peak-to-peak ratio: interneurons have a large peak value after the valley point, while pyramidal cells usually have a flatter waveform with smaller peaks and smaller peak-to-peak value (Viskontas et al., 2007).

Slice electrophysiological recording *in vitro*
The day after modeling, mice (5 per group) were anesthetized with avertin solution and decapitated. Slice preparation and electrophysiological recording were performed as described previously (Yao et al., 2018b). Briefly, the brains were quickly removed and the infarcted hemisphere (right side) was discarded. The contralateral hemisphere (left side) containing the S1 and M1 was placed in ice-cold cutting solution (aCSF; Sigma-Aldrich) containing 110 mM choline chloride, 7 mM $MgSO_4$, 2.5 mM KCl, 1.25 mM NaH_2PO_4, 25 mM $NaHCO_3$, 25 mM D-glucose, 11.6 mM sodium ascorbate, 3.1 mM sodium pyruvate, and 0.5 mM $CaCl_2$ and gassed with 95% O_2 and 5% CO_2. Coronal sections (slice thickness, 400 μm) were cut on a VT1200S vibratome (Leica, Wetzlar, Germany) in cutting solution at 4°C. Slices were allowed to recover for 30 minutes at 32°C and then transferred to a self-made holding chamber at room temperature for solution containing 127 mM NaCl, 2.5 mM KCl, 1.25 mM NaH_2PO_4, 25 mM $NaHCO_3$, 25 mM D-glucose, 2 mM $CaCl_2$, and 1 mM $MgSO_4$. Recording started 1 hour after recovery and lasted for 4 hours. Individual slices were observed under an upright microscope (Eclipse FN1; Nikon, Tokyo, Japan) with a ×40 water-immersion differential interference contrast objective and screened on a digital complementary metal oxide semiconductor camera (C11440-42U; Hamamatsu Photonics, Hamamatsu, Japan). On average, 3 to 4 slices per mouse were constantly perfused at room temperature (23–26°C) with oxygenated incubation solution (4–5 mL/min). Recordings were made from M1 and S1 neurons located in both Layer 2/3 and Layer 5/6.

For action potential recording, recording pipettes with 4–8 MΩ were filled with electrode internal solution containing 128 mM K-Gluconate, 10 mM NaCl, 2 mM $MgCl_2$, 0.5 mM EGTA, 10 mM HEPES, 4 mM Na_2ATP, and 0.4 mM Na_2GTP. To explore synaptic transmission, spontaneous excitatory post synaptic currents (sEPSCs) were recorded at –60 mV using a voltage clamp. The internal solution contained 125 mM $CsMeSO_4$, 5 mM NaCl, 1.1 mM EGTA, 10 mM HEPES, 0.3 mM Na_2GTP, 4 mM Mg-ATP, and 5 mM QX-314. Pyramidal neurons characterized by their apical dendrite and triangular somata were selected for recording. Data were acquired using a Multiclamp 700B amplifier and a Digidata 1550B acquisition system (Molecular Devices, San Jose, CA, USA). The sampling rate was set at 10 kHz and signals were filtered at 2 kHz. If series resistance was over 30MΩ, the data were excluded.

To detect intrinsic excitability, action potentials were induced by 500 ms current steps (20 pA increments from –100 pA to 500 pA). Resting membrane potential was measured using a current clamp without a current injection. Input resistance was analyzed using a test pulse with 5 mV injection. Action potential threshold was measured as the membrane potential that caused single action potential firing. Spike number was counted at 300 pA current injection. For analysis of sEPSCs, amplitude and frequency were calculated using the Mini Analysis Program software (Synaptosoft Inc., Decatur, GA, USA).

Cerebral stereotactic injection
The Alexa Fluor retrograde cholera toxin B (CTB488) tracer was used to trace the structural connection between bilateral S1 and injection site M1 (neurons in M1 projecting from S1) in mice (**Figure 2D**). CTB488 (1 μg/μL; BrainVTA, Wuhan, Hubei Province, China) was injected into left M1. Five days after the injection, the mice were anesthetized with avertin solution and decapitated. After brain slicing (see the immunofluorescence part), the number of CTB488-positive neurons projecting from bilateral S1 to M1 were counted using ImageJ software version 1.53c (National Institutes of Health, Bethesda, MD, USA).

To further test the function of contralateral S1 in EA-mediated recovery after M1 infarction, we ablated the neurons using viral infection. For neuronal ablation, rAAV-hsyn-taCasp3-TEVp-p2A-EGFP-WRPEs virus (300 nL with a titer of 2.72 × 10^{12} vg/mL; BrainVTA) was injected into the left S1 (Yao et al., 2018a), and rAAV-hsyn-taCasp3-p2A-EGFP-WRPEs virus (300 nL with a titer of 2.60 × 10^{12} vg/mL; BrainVTA) was used for control. Three weeks after virus injection, *in vivo* recording and blood perfusion testing was performed.

Immunofluorescence
To confirm the structural connection between S1 and M1 (**Figure 2D**) and the efficacy of virus-induced neuronal ablation, 13 mice injected with CTB488 tracer and virus were anesthetized with avertin and then perfused with saline followed by 4% paraformaldehyde (PFA) (Mubiotech, Shanghai, China). The brains were fixed overnight in 4% PFA and dehydrated with 15% and 30% sucrose. Brains were

sectioned (slice thickness, 40 μm) using a sliding freezing microtome (Leica 819; Leica Biosystems, Buffalo Grove, IL, USA). Sections were washed in phosphate-buffered saline (PBS) (Thermo Fisher Scientific, Waltham, MA, USA), and then incubated in blocking solution (10% BSA, Macklin, China; 0.3% Triton X-100, Biosharp, China), and incubated overnight at 4°C with primary antibody to NeuN (Anti-NeuN antibody, Mouse Monoclonal Antibody, Millipore, USA, Cat# MAB377; dilution 1:500). The next day, sections were washed with PBS and incubated for 2 hours at room temperature with secondary antibody (goat anti-mouse, IgG conjugated to Alexa Fluor 594, Abcam, UK, Cat# ab150116; dilution 1:500). Finally, sections were washed in PBS, incubated with 4,6-diamidino-2-phenylindole (DAPI; Sigma-Aldrich; diluted 1:5000, stock solution 1 mg/mL) for staining of nuclei.

To observe neuronal staining in the CTB tracing experiments and confirm the efficacy of S1 ablation, the sections from mice with CTB tracer or virus injection after immunofluorescence staining were further imaged. Confocal fluorescence images detecting neuronal staining were acquired on a confocal microscope using ×20 and ×40 air objectives (Nikon). Image analysis was performed using either ImageJ software version 1.53c for counting analysis or NIS-Viewer version 4.5 (Nikon). Cell density was calculated from a total of 10 sections and every 2 sections were included for each mouse (**Table 1**). Cells were counted in a blinded manner.

Table 1 | Animal assignment in each expeirment

	Determination	Group	Number of mice	Time point
Figure 2	Blood perfusion	Sham	5	Within 24 h
		Stroke	5	
		Stroke + EA	5	
	Coherence test	Sham	5	Within 24 h
		Stroke	5	
		Stroke + EA	5	
	CTB experiment	Wild-type	3	5 d after virus injection
Figure 3	Slice recording in M1	Sham	5	Within 24 h
		Stroke	5	
		Stroke + EA	5	
Figure 4	Slice recording in S1	Sham	5	Within 24 h
		Stroke	5	
		Stroke + EA	5	
Figure 5	*In vivo* recording	Sham	5	Within 24 h
		Stroke	5	
		Stroke + EA	5	
Figure 6	taCasp3 virus experiments	Wild-type-control	5	21 d after virus injection
		Wild-type-ablation	5	
	In vivo recording after virus injection	Sham	5	Within 24 h
		Stroke	5	
		Stroke + EA	5	
	Blood perfusion after control virus (taCasp3-EGFP) injection	Sham	5 (entire brain), 5 (contralateral M1 and S1)	Within 24 h
		Stroke	5 (entire brain), 5 (contralateral M1 and S1)	
		Stroke + EA	8 (entire brain), 5 (contralateral M1 and S1)	
	Blood perfusion after ablation virus (taCasp3-TEVp) injection	Sham	5 (entire brain), 5 (contralateral M1 and S1)	Within 24 h
		Stroke	6 (entire brain), 5 (contralateral M1 and S1)	
		Stroke + EA	5 (entire brain), 5 (contralateral M1 and S1)	

EA: Electroacupuncture; EGFP: enhanced green fluorescent protein.

Statistical analysis

No statistical methods were used to predetermine sample size; however, our sample sizes are similar to those reported in previous publications (Cui et al., 2018). Electrophysiological recordings and their analysis were blinded to genotype and treatment, whereas *in vivo* microscopy and analysis were not. Twelve mice died after stroke induction, therefore, the remaining 38 stroke mice received EA treatment and were used for further analysis. Data were analyzed using one-way analysis of variance with *post hoc* Bonferroni correction or the unpaired *t*-test. Data are presented as means with standard error of the mean. All statistical analyses were performed using GraphPad Prism software version 7.0 (GraphPad Software Inc., San Diego, CA, USA). $P < 0.05$ was considered significant.

Results

The interaction between contralateral M1 and S1 is impaired after unilateral focal ischemia in M1 and acute EA rescues this impairment

The decrease in blood perfusion of the entire brain, M1, and S1 following stroke induction was significantly rescued by EA at acupoints GV14 and GV20 ($P < 0.01$) (**Figure 2A–C** and **Additional Figures 1** and **2**). To confirm the structural connection between bilateral S1 and M1 after M1 infarction, CTB488 tracer was injected into left M1. CTB-488-positive neurons were obviously observed in S1 (**Figure 2D**). Interestingly, we also found CTB488-positive neurons in contralateral S1. The number of CTB488-positive neurons between the ipsilateral and contralateral S1 did not differ ($P > 0.05$) (**Additional Figure 3**). This demonstrated monosynaptic projection from S1 to M1. To further explore the functional connection between the contralateral M1 and S1, we evaluated coherence between S1 and M1 by recording neuronal activity in these two regions simultaneously *in vivo*. Compared with the sham group, the coherence between S1 and M1 was greatly disturbed in the stroke group ($P < 0.01$). EA at GV14 and GV20 acupoints inhibited this attenuation ($P < 0.05$) (**Figure 2E**).

The effect of EA on intrinsic excitability of neurons located in Layer 2/3 and Layer 5/6 in contralateral M1 and S1 determined by slice electrophysiological recording

To further explore the role of neuronal activity in the effect mechanism of EA treatment, we evaluated neuronal intrinsic excitability using *in vitro* slice electrophysiological recording. The excitability parameters analyzed included resting membrane potential, input resistance, action potential threshold, and the number of spikes induced by 300 pA current injection. Since excitatory neurons account for approximately 80% of neurons in the brain, we targeted excitatory neurons for recording in both Layer 2/3 and Layer 5/6 of M1. Compared to the sham group, the measured parameters did not differ in the stroke or stroke + EA groups (**Figure 3**). Neurons located in Layer2/3 and Layer5/6 of S1 were further recorded in parallel. The resting membrane potential, input resistance, and action potential threshold showed no change after stroke or EA treatment in either Layer 2/3 or Layer 5/6. (**Figure 4**). However, the number of spikes induced by 300pA current injection in neurons located in Layer 5/6 was significantly higher in the stroke group than the sham group ($P < 0.01$). This enhanced excitability was absent in the stroke + EA group ($P < 0.05$) compared to the stroke group, suggesting the enhanced intrinsic excitability in Layer 5/6 of contralateral S1 can be recovered by EA treatment (**Figure 4-B4**). After further studying synaptic transmission in contralateral S1, neither amplitude nor frequency of sEPSCs in S1 was changed in Layer 2/3 or Layer 5/6 (**Additional Figure 4**).

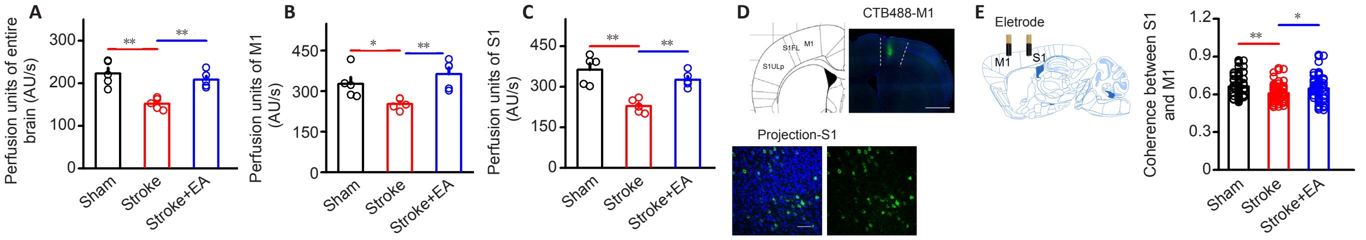

Figure 2 | EA improves cerebral blood perfusion and S1-M1 coherence in mice within 24 hours of unilateral focal photothrombotic infarct in M1.
(A–C) Blood perfusion was detected using laser speckle blood flow imaging. Blood perfusion of the entire brain (A), contralateral M1 (B), and S1 (C) after stroke was rescued by EA treatment. (D) Five days after CTB488 injection, CTB488-positive neurons in S1 (green) projected from M1. CTB-488 was injected into M1 of wild-type control mice. Blue: DAPI. A confocal microscope was used to detect CTB488-positive neurons. Scale bars: 50 µm. (E) Neuronal activity of contralateral S1 and M1 was simultaneously recorded to analyze coherence. The coherence relationship between S1 and M1 after stroke was enhanced by EA treatment. All experiments were repeated five times. Data are presented as means ± standard error of the mean (see Table 1 for the number of mice used in Figure 2). Number of units = 96 in the sham, stroke, and stroke + EA groups, respectively. Units were categorized as neuronal clusters with different discharge frequency and waveforms. *P < 0.05, **P < 0.01 (one-way analysis of variance with *post hoc* Bonferroni correction). CTB: Cholera Toxin Subunit B; EA: electroacupuncture; M1: primary motor cortex; S1: primary somatosensory cortex.

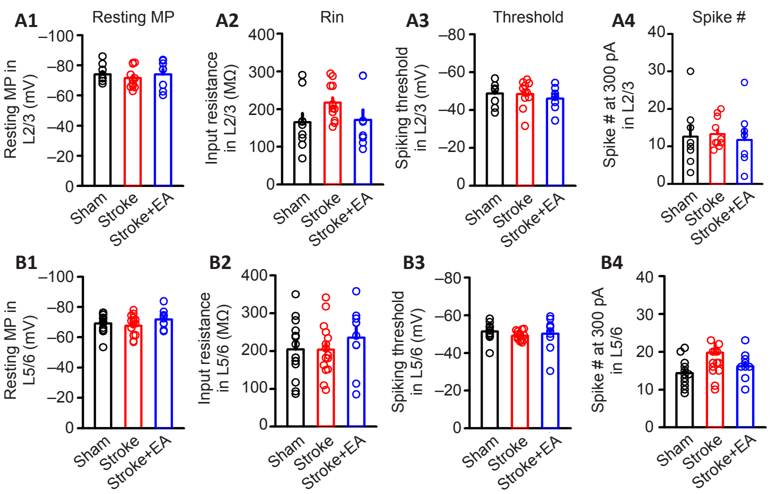

Figure 3 | Intrinsic excitability of neurons located in the contralateral M1 in Layer 2/3 and Layer 5/6 was detected by slice electrophysiological recording within 24 hours of unilateral focal photothrombotic infarct in M1.
In Layer2/3 neurons, the resting membrane potential (Resting MP) (A1), input resistance (Rin) (A2), threshold to spike (A3) and spike number induced at 300 pA current injection (Spike #) (A4) were not significantly different between the sham, stroke, and stroke + EA groups. Number of neurons = 9, 12, and 8 in the sham, stroke and stroke + EA groups, respectively. (B1–B4) Similar to the results in Layer 2/3, the resting membrane potential (B1), input resistance (B2), threshold to spike (B3), and spike number induced at 300pA current injection (B4) in Layer 5/6 neurons were not affected by stroke or EA. All experiments were repeated five times. Data are presented as means ± standard error of the mean (see Table 1 for the number of mice used in Figure 3). Number of neurons = 14, 15, and 10 in the sham, stroke, and stroke + EA groups, respectively. EA: Electroacupuncture; L2/3: Layer 2/3; L5/6: Layer 5/6.

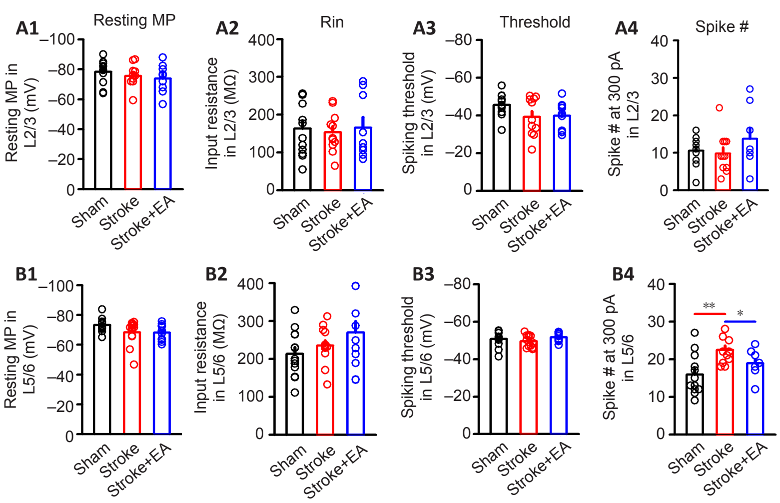

Figure 4 | Excitability in Layer 2/3 and Layer 5/6 neurons located in contralateral S1 was demonstrated using *in vitro* slice electrophysiological recording within 24 hours of unilateral focal photothrombotic infarct in M1.
(A1–A4) The resting membrane potential (resting MP) (A1), input resistance (Rin) (A2), threshold to spike (A3), and number of spikes induced at 300 pA current injection (Spike #) (A4) was not significantly different among the sham, stroke, and stroke + EA groups in Layer 2/3. Number of neurons = 12, 11, and 9 in the sham, stroke, and stroke + EA groups, respectively. (B1–B4) In Layer 5/6, the resting membrane potential (B1), input resistance (B2), and threshold to spike (B3) were not affected by stroke or EA treatment. However, the number of spikes induced at 300 pA current injection was significantly higher in the stroke group than the sham group (P < 0.01) but significantly lower in the stroke + EA group than the stroke group (P < 0.05). Number of neurons = 13, 12, and 11 in the sham, stroke, and stroke + EA groups, respectively. All experiments were repeated at least five times. Data are presented as meana ± standard error of the mean. See Table 1 for the number of mice used in Figure 4. *P < 0.05, **P < 0.01 (one-way analysis of variance with *post hoc* Bonferroni correction). EA: Electroacupuncture; L2/3: Layer 2/3; L5/6: Layer 5/6.

EA treatment increases stroke-induced impaired neuronal activity in Layer 5/6 in both the contralateral M1 and S1 *in vivo*

The above results showed that activity in Layer 2/3 showed no change *in vitro* (**Figures 3A** and **4A**). Considering these results, and that spontaneous neuronal activity in Layer 2/3 is sparse in acute electrophysiological recording manipulation (Crochet et al., 2011; Barth and Poulet, 2012), we focused our *in vivo* recordings on firing rate and waveform of interneurons and pyramidal neurons in Layer 5/6. Excitatory neuronal activity in the contralateral M1 and S1 of Layer 5/6 was significantly lower in the stroke group than the sham group (P < 0.05 and P < 0.01, respectively). In the stroke + EA group, neuronal activity was significantly higher in both contralateral M1 and S1 of Layer 5/6 compared with the stroke group (P < 0.01 and P < 0.05, respectively; **Figure 5**). Inhibitory neuronal activity in S1 and M1 showed impairment in the stroke group compared to the sham group (P < 0.01 and P < 0.05, respectively). This impairment was recovered to some extent in the stroke + EA group (**Additional Figure 5**).

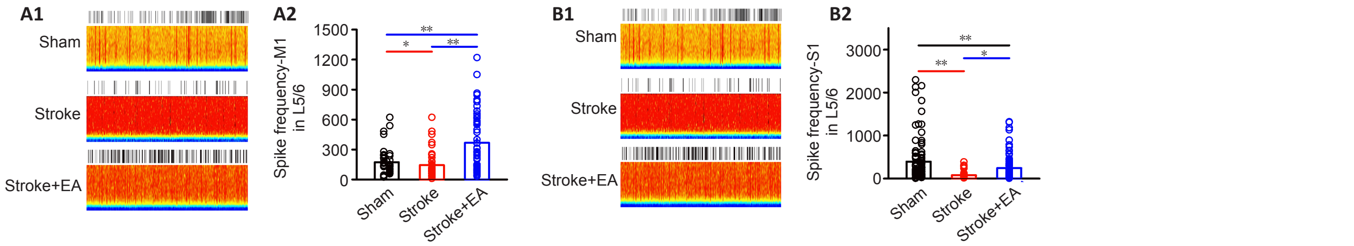

Figure 5 | EA increases neuronal firing in the contralateral M1 and S1 within 24 hours of unilateral focal photothrombotic infarct in M1 (electrophysiological recording *in vivo*).
Samples showing raster and spectrum for spike firing (A1 and B1). Time showed is 300 seconds. Impairment of spike frequency induced by stroke was rescued by electroacupuncture treatment in Layer 5/6 of both M1 (A2) and S1 (B2). For M1: number of units = 44, 43, and 53 for the sham, stroke, and stroke + EA groups, respectively. For S1: number of units = 103, 44, and 107 for the sham, stroke, and stroke + EA groups, respectively. All experiments were repeated five times. Data are presented as means ± standard error of the mean. See Table 1 for the number of mice used in Figure 5. **P* < 0.05, ***P* < 0.01 (one-way analysis of variance with *post hoc* Bonferroni correction). EA: Electroacupuncture; L5/6: Layer 5/6.

Disturbing neuronal function in contralateral S1 blocks the efficacy of EA

The neurons in S1 were significantly ablated in the taCasp3-TEVp group compared with the taCasp3-EGFP group (*P* < 0.05; **Figure 6A**). After S1 ablation, impairment of neuronal activity (including excitatory and inhibitory neurons) in M1 caused by stroke induction was absent and EA treatment showed no efficacy (**Figure 6B** and **Additional Figure 6**). This suggests that S1 function is crucial for modulating neuronal activity in M1.

In the control group (rAAV-hsyn-taCasp3-p2A-EGFP-WRPEs virus injection), blood perfusion of the entire brain was significantly lower in the stroke group than the sham group (*P* < 0.01) but significantly higher in the stroke + EA group than the stroke group (*P* < 0.01; **Figure 6C**). Local M1 and S1 perfusion showed similar changes among the groups (**Figure 6D** and **E**). However, after ablation, although the blood perfusion was significantly lower in the stroke group (*P* < 0.01 or *P* < 0.05), blood perfusion recovery mediated by EA at GV14 and GV20 disappeared in the entire brain, contralateral M1, and S1 (**Figure 6C–E**).

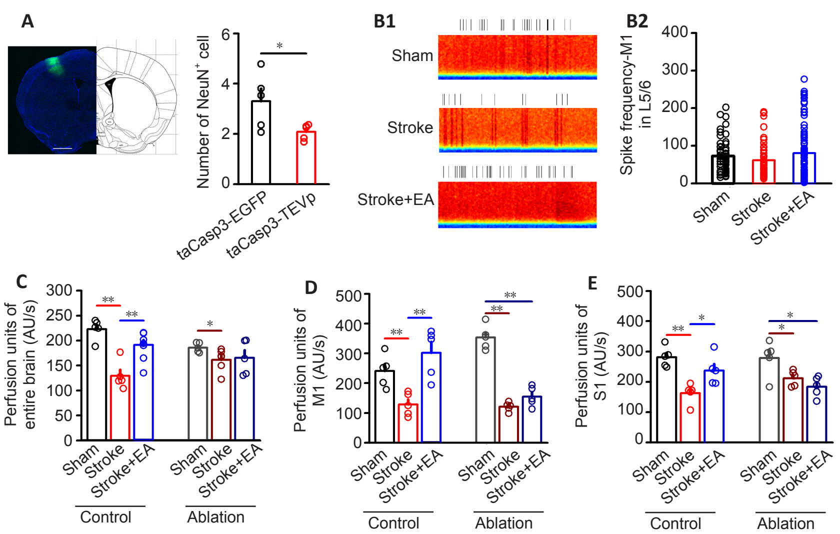

Figure 6 | After S1 ablation, EA treatment at GV14 and GV20 does not enhance neuronal activity or blood perfusion of contralateral M1 and S1 within 24 hours of unilateral focal photothrombotic infarction in M1.
(A) taCasp3 virus (including rAAV-hsyn-taCasp3-TEVp-p2A-EGFP-WRPEs and rAAV-hsyn-taCasp3-p2A-EGFP-WRPEs) were injected into contralateral S1. The density of $NeuN^+$ neurons was measured within the infected area. The number of $NeuN^+$ neurons was ablated significantly in the taCasp3-TEVp group compared with the taCasp3-EGFP group (*P* < 0.05). Green, neurons expressing the taCasp3-EGFP virus; Blue, DAPI. (B1) Samples showing raster and spectrum in spike continuous in M1 after S1 ablation. Time shown is 300 seconds. (B2) Spike frequency in Layer 5/6 in M1 was not significantly different between the groups after S1 ablation. Number of units = 57, 51, and 83 in the sham, stroke, and stroke + EA groups. (C) EA treatment lost its efficacy with respect to blood perfusion of the entire brain after S1 ablation. (D) EA treatment lost its efficacy with respect to blood perfusion of the contralateral M1 after S1 ablation. (E) EA treatment lost its efficacy with respect to blood perfusion of the contralateral S1 after S1 ablation. All experiments were repeated at least five times. Data are presented as means ± standard error of the mean. **P* < 0.05, ***P* < 0.01 (unpaired t-test in A, and one-way analysis of variance with *post hoc* Bonferroni correction in B–E). CTB: Cholera Toxin Subunit B; EA: electroacupuncture.

Discussion

In this study, EA at GV20 and GV14 rescued stroke-induced impairment of blood perfusion and neuronal activity in the contralateral M1 and S1. Moreover, coherence between the contralateral S1 and M1 was disturbed after stroke, which was improved after EA. We further demonstrated that *in vivo* neuronal activity in both M1 and S1 was decreased after stroke. Although intrinsic excitability of neurons in the contralateral M1 showed no change after stroke or EA treatment, the excitability in Layer 5/6 of S1 showed enhancement after stroke, which could be rescued by EA. Virus-mediated ablation of neurons in the contralateral S1 inhibited the therapeutic effect of EA. Our results indicate that neuronal activity of the contralateral S1 is important for EA-mediated recovery after focal M1 infarction. EA treatment, which is safe, low-cost, and easily accessible, can modulate contralateral hemispheric compensation of impaired brain function. Furthermore, our study provides insight into how neural circuits can be influenced by EA in central nervous system disorders.

Sensory processing, including temporal coding ipsilateral to the infarction site, has been reported to be disturbed in cerebral infarction (Fukui et al., 2020). Our study provides evidence of unilateral M1 infarction causing dysfunction of the contralateral S1. Numerous reports have shown that contralateral brain regions experience structural and functional plasticity after stroke (Cramer and Crafton, 2006; Cramer, 2008). Our results indicate that coherence between contralateral M1 and S1 is impaired. Sensory deficit caused by M1 infarction has been shown in both rodent and primate studies (Johansson and Cole, 1992; Nudo et al., 2000; Friel et al., 2005). Therefore, after unilateral photothrombotic M1 infarction, reorganization and neural plasticity can occur in the ipsilateral S1 (Fukui et al., 2020). For the interhemispheric interaction, it is plausible that neuronal change in the ipsilateral S1 likely affects neuronal activity in the contralateral S1 (Murase et al., 2004). Another recent study indicated that coherence of the motor and the sensory cortex after stroke is impaired in the ipsilateral side relative to the contralateral hemisphere (Mohammadzadeh et al., 2020). Our study further suggests that coherence in the contralateral hemisphere is dysfunctional. Future studies of EA-mediated changes in interactions and functional connectivity between the contralateral S1 and ipsilateral S1 after stroke are warranted.

Neuronal excitability differed between *in vivo* and *in vitro* electrophysiological recordings in our study. We suggest several possible explanations. First, neuronal excitability is determined by two factors, synaptic input and intrinsic excitability (vanVreeswijk and Sompolinsky, 1996). Our *in vivo* data demonstrated decreased neuronal activity, which may be mostly attributable to impaired synaptic input; however, *in vitro*, this input has been disconnected. Second, increased intrinsic excitability may have compensated for decreased neuronal activity. Our *in vivo* results are in line with a previous report that showed *in vivo* impairment of neuronal activity in the contralateral M1 (Cui et al., 2020). Moreover, our *in vitro* finding of increased intrinsic excitability is consistent with previous *in vitro* results (Kubis, 2016; Zhu et al., 2017; Afzal et al., 2019). A previous study showed that the GABAergic circuit marker was lost during stroke recovery (Bavelier et al., 2010). However, Paz et al. (2010) reported that intrinsic excitability was decreased in the reticular thalamus nucleus after focal somatosensory cortical injuries in 3-week old rats at the end of the first week. This discrepancy might be attributed to the different time points of detection after stroke, the different brain regions explored, or differences in age of the mice studied. One limitation of our study is that the changes were detected only in the acute stroke stage. The effect of long-term EA treatment on neuronal activity and neural circuits during stroke recovery still needs to be examined.

Previous structural and physiological studies have suggested that sensory information is relayed by the thalamus, which projects input to Layer 4 up to Layer 2/3 and down to Layer 5 in S1 (Douglas and Martin, 2004). It is thought that S1 has reciprocal connections with M1. The M1–S1 circuit neurons in S1 are located in Layer 2/3 and Layer 5a and connect with neurons in Layer 2/3 and Layer 5a of M1 (Edwards et al., 2019). Although our *in vitro* data demonstrated that the excitability of neurons in Layer 2/3 in both the contralateral S1 and M1 showed no change after stroke, neuronal activity in Layer 5/6 of the contralateral S1 was impaired after the focal M1 infarction; ablating the contralateral S1 activity abolished the EA-mediated recovery in blood perfusion. Tennant et al. (2017) reported that chronic optogenetic activation input from the thalamus to S1 could promote recovery after stroke. Thalamic input to the contralateral S1 should be further explored in future studies.

In conclusion, this study explored the acute effect of EA at GV20 and GV14 on neuronal activity and interaction between S1 and M1. Our results provide insight into the mechanism underlying EA regulation of neural circuitry after stroke. Future studies should further explore the underlying mechanism of alterations in intrinsic excitability and how the interaction between cortical and subcortical brain regions is disrupted. In addition, further study of how inhibitory neurons in the contralateral hemisphere contributes to stroke pathogenesis and recovery is also warranted.

Author contributions: *Experiment design, data collection and analysis and manuscript writing: LLY; experiment design, data collection and analysis: SY, ZNW, JYL, XRT, CZT; experiment design, data collection and manuscript writing: SC; experiment design, data analysis, and manuscript writing: NGX. All authors the final version of this manuscript for publication.*
Conflicts of interest: *The authors declare that they have no conflict of interest.*
Financial support: *This work was supported by Guangzhou University of Chinese Medicine and by grants from General Program of the National Natural Science Foundation of China (No. 81774406, to NGX), Youth Program of the National Natural Science Foundation of China (No. 82004469, to LLY), Fellowship of China postdoctoral Science Foundation (No. 2020M672601, to LLY), Opening Operation Program of Key Laboratory of Acupuncture and Moxibustion of Traditional Chinese Medicine in Guangdong (No. 2017B030314143, to NGX). The funding sources had no role in study conception and design, data analysis or interpretation, paper writing or deciding to submit this paper for publication.*
Institutional review board statement: *All animal surgery procedures were approved by the Committee for Care and Use of Research Animals of Guangzhou University of Chinese Medicine (approval No. 20200407009) April 7, 2020.*
Copyright license agreement: *The Copyright License Agreement has been signed by all authors before publication.*
Data sharing statement: *Datasets analyzed during the current study are available from the corresponding author on reasonable request.*
Plagiarism check: *Checked twice by iThenticate.*
Peer review: *Externally peer reviewed.*

Additional files:
Additional Figure 1: *Laser speckle blood flow imaging showed blood perfusion in the entire brain was decreased after stroke, while rescued by EA.*
Additional Figure 2: *The time course of perfusion blood in the entire brain in mice.*
Additional Figure 3: *Cell density of CTB488-positive neurons in the bilateral hemispheric S1 labeled by CTB tracer.*
Additional Figure 4: *The neuronal synaptic transmission in Layer 2/3 and Layer 5/6 located contralateral S1 is not altered after stroke or EA treatment.*
Additional Figure 5: *The activity of inhibitory neurons in Layer 5/6 located contralateral M1 and S1 is decreased after stroke, while this impairment is not thoroughly rescued by EA treatment.*
Additional Figure 6: *The inhibitory neuronal activity in vivo in Layer 5/6 located contralateral M1 is not changed after stroke induction or EA treatment after S1 ablation.*

References

Afzal T, Chardon MK, Rymer WZ, Suresh NL (2019). Stretch reflex excitability in contralateral limbs of stroke survivors is higher than in matched controls. J Neuroeng Rehabil 16:154.
Bai L, Cui F, Zou Y, Lao L (2013) Acupuncture de qi in stable somatosensory stroke patients: relations with effective brain network for motor recovery. Evid Based Complement Alternat Med 2013:197238.
Barth AL, Poulet JF (2012) Experimental evidence for sparse firing in the neocortex. Trends Neurosci 35(6):345-355.
Bartho P, Hirase H, Monconduit L, Zugaro M, Harris KD, Buzsaki G (2004) Characterization of neocortical principal cells and Interneurons by network interactions and extracellular features. J Neurophysiol 92:600-608.
Bavelier D, Levi DM, Li RW, Dan Y, Hensch TK (2010) Removing Brakes on Adult Brain Plasticity: From Molecular to Behavioral Interventions. J Neurosci 30:14964-14971.
Bolognini N, Russo C, Edwards DJ (2016) The sensory side of post-stroke motor rehabilitation. Restor Neurol Neurosci 34:571-586.
Borich MR, Brodie SM, Gray WA, Ionta S, Boyd LA (2015) Understanding the role of the primary somatosensory cortex: Opportunities for rehabilitation. Neuropsychologia 79:246-255.
Buetefisch CM (2015) Role of the contralesional hemisphere in post-stroke recovery of upper extremity motor function. Front Neurol 6:214.
Calautti C, Baron JC (2003) Functional neuroimaging studies of motor recovery after stroke in adults: a review. Stroke 34:1553-1566.
Chang QY, Lin YW, Hsieh CL (2018) Acupuncture and neuroregeneration in ischemic stroke. Neural Regen Res 13:573-583.
Chavez LM, Huang SS, MacDonald I, Lin JG, Lee YC, Chen YH (2017) Mechanisms of acupuncture therapy in ischemic stroke rehabilitation: a literature review of basic studies. Int J Mol Sci 18:2270.

Cheng CY, Lin JG, Tang NY, Kao ST, Hsieh CL (2014) Electroacupuncture-like stimulation at the Baihui (GV20) and Dazhui (GV14) acupoints protects rats against subacute-phase cerebral ischemia-reperfusion injuries by reducing S100B-mediated neurotoxicity. PLoS One 9:e91426.
Cramer SC (2008) Repairing the human brain after stroke. II. Restorative therapies. Ann Neurol 63:549-560.
Cramer SC (2018) Treatments to promote neural repair after stroke. J Stroke 20:57-70.
Cramer SC, Crafton KR (2006) Somatotopy and movement representation sites following cortical stroke. Exp Brain Res 168:25-32.
Crochet S, Poulet JF, Kremer Y, Petersen CC (2011) Synaptic mechanisms underlying sparse coding of active touch. Neuron 69:1160-1175.
Csicsvari J, Hirase H, Czurko A, Buzsaki G (1998) Reliability and state dependence of pyramidal cell-interneuron synapses in the hippocampus: an ensemble approach in the behaving rat. Neuron 21:179-189.
Csicsvari J, Hirase H, Czurko A, Mamiya A, Buzsaki G (1999) Oscillatory coupling of hippocampal pyramidal cells and interneurons in the behaving rat. J Neurosci 19:274-287.
Cui S, Wang K, Wu SB, Zhu GQ, Cao J, Zhou YP, Zhou MQ (2018) Electroacupuncture modulates the activity of the hippocampus-nucleus tractus solitarius-vagus nerve pathway to reduce myocardial ischemic injury. Neural Regen Res 13:1609-1618.
Cui S, Yao SQ, Wu CX, Yao LL, Huang PD, Chen YJ, Tang CZ, Xu NG (2020) Electroacupuncture involved in motor cortex and hypoglossal neural control to improve voluntary swallowing of poststroke dysphagia mice. Neural Plast 2020:8857543.
Dancause N, Nudo RJ (2011) Shaping plasticity to enhance recovery after injury. Prog Brain Res 192:273-295.
Douglas RJ, Martin KA (2004) Neuronal circuits of the neocortex. Annu Rev Neurosci 27:419-451.
Edwards LL, King EM, Buetefisch CM, Borich MR (2019) Putting the “Sensory” into sensorimotor control: the role of sensorimotor integration in goal-directed hand movements after stroke. Front Integr Neurosci 13:16.
Friel KM, Barbay S, Frost SB, Plautz EJ, Hutchinson DM, Stowe AM, Dancause N, Zoubina EV, Quaney BM, Nudo RJ (2005) Dissociation of sensorimotor deficits after rostral versus caudal lesions in the primary motor cortex hand representation. J Neurophysiol 94:1312-1324.
Fukui A, Osaki H, Ueta Y, Kobayashi K, Muragaki Y, Kawamata T, Miyata M (2020) Layer-specific sensory processing impairment in the primary somatosensory cortex after motor cortex infarction. Sci Rep 10:3771.
Gonzalez CLR, Gharbawie OA, Williams PT, Kleim JA, Kolb B, Whishaw IQ (2004) Evidence for bilateral control of skilled movements: ipsilateral skilled forelimb reaching deficits and functional recovery in rats follow motor cortex and lateral frontal cortex lesions. Eur J Neurosci 20:3442-3452.
Hatem SM, Saussez G, Della Faille M, Prist V, Zhang X, Dispa D, Bleyenheuft Y (2016) Rehabilitation of motor function after stroke: a multiple systematic review focused on techniques to stimulate upper extremity recovery. Front Hum Neurosci 10:442.
Hiraba H, Yamaguchi Y, Satoh H, Ishibashi Y, Iwamura Y (2000) Deficits of masticatory movements caused by lesions in the orofacial somatosensory cortex of the awake cat. Somatosens Mot Res 17:361-372.
Johansson BB (2011) Current trends in stroke rehabilitation. A review with focus on brain plasticity. Acta Neurol Scand 123:147-159.
Johansson RS, Cole KJ (1992) Sensory-motor coordination during grasping and manipulative actions. Curr Opin Neurobiol 2:815-823.
Kim YR, Kim HN, Ahn SM, Choi YH, Shin HK, Choi BT (2014) Electroacupuncture promotes post-stroke functional recovery via enhancing endogenous neurogenesis in mouse focal cerebral ischemia. PLoS One 9:e90000.
Kinnischtzke AK, Fanselow EE, Simons DJ (2016) Target-specific M1 inputs to infragranular S1 pyramidal neurons. J Neurophysiol 116:1261-1274.
Kubis N (2016) Non-invasive brain stimulation to enhance post-stroke recovery. Front Neural Circuits 10:56.
Li Z, Yang M, Lin Y, Liang S, Liu W, Chen B, Huang S, Li J, Tao J, Chen L (2021) Electroacupuncture promotes motor function and functional connectivity in rats with ischemic stroke: an animal resting-state functional magnetic resonance imaging study. Acupunct Med 39:146-155.
Liang H, Zhao H, Gleichman A, Machnicki M, Telang S, Tang S, Rshtouni M, Ruddell J, Carmichael ST (2019) Region-specific and activity-dependent regulation of SVZ neurogenesis and recovery after stroke. Proc Natl Acad Sci U S A 116:13621-13630.
Lu L, Zhang XG, Zhong LL, Chen ZX, Li Y, Zheng GQ, Bian ZX (2016) Acupuncture for neurogenesis in experimental ischemic stroke: a systematic review and meta-analysis. Sci Rep 6:19521.
Mathis MW, Mathis A, Uchida N (2017) Somatosensory cortex plays an essential role in forelimb motor adaptation in mice. Neuron 93:1493-1503.e6.
Mohammadzadeh L, Latifi H, Khaksar S, Feiz MS, Motamedi F, Asadollahi A, Ezzatpour M (2020) Measuring the frequency-specific functional connectivity using wavelet coherence analysis in stroke rats based on intrinsic signals. Sci Rep 10:9429.
Murase N, Duque J, Mazzocchio R, Cohen LG (2004) Influence of interhemispheric interactions on motor function in chronic stroke. Ann Neurol 55:400-409.
Murphy TH, Corbett D (2009) Plasticity during stroke recovery: from synapse to behaviour. Nat Rev Neurosci 10:861-872.
Nudo RJ, Friel KM, Delia SW (2000) Role of sensory deficits in motor impairments after injury to primary motor cortex. Neuropharmacology 39:733-742.
Park YW, Heo GY, Kim MJ, Lee SY, Choi BT, Shin HK (2019) Subacute electroacupuncture at Baihui (GV 20) and Dazhui (GV 14) promotes post-stroke functional recovery via neurogenesis and astrogliosis in a photothrombotic stroke mouse model. J Tradit Chin Med 39:833-841.
Pavlides C, Miyashita E, Asanuma H (1993) Projection from the sensory to the motor cortex is important in learning motor skills in the monkey. J Neurophysiol 70:733-741.
Paxinos G, Franklin KBJ (2013) Paxinos and Franklin’s the mouse brain in stereotaxic coordinates. 4th ed. Boston: Elsevier/Academic Press.
Petrof I, Viaene AN, Sherman SM (2015) Properties of the primary somatosensory cortex projection to the primary motor cortex in the mouse. J Neurophysiol 113:2400-2407.
Reinecke S, Dinse HR, Reinke H, Witte OW (2003) Induction of bilateral plasticity in sensory cortical maps by small unilateral cortical infarcts in rats. Eur J Neurosci 17:623-627.
Sachidhanandam S, Sreenivasan V, Kyriakatos A, Kremer Y, Petersen CC (2013) Membrane potential correlates of sensory perception in mouse barrel cortex. Nat Neurosci 16:1671-1677.
Si QM, Wu GC, Cao XD (1998) Effects of electroacupuncture on acute cerebral infarction. Acupunct Electrother Res 23:117-124.
Takatsuru Y, Fukumoto D, Yoshitomo M, Nemoto T, Tsukada H, Nabekura J (2009) Neuronal circuit remodeling in the contralateral cortical hemisphere during functional recovery from cerebral infarction. J Neurosci 29:10081-10086.
Tennant KA, Taylor SL, White ER, Brown CE (2017) Optogenetic rewiring of thalamocortical circuits to restore function in the stroke injured brain. Nat Commun 8:15879.
vanVreeswijk C, Sompolinsky H (1996) Chaos in neuronal networks with balanced excitatory and inhibitory activity. Science 274:1724-1726.
Vecchia D, Beltramo R, Vallone F, Chereau R, Forli A, Molano-Mazon M, Bawa T, Binini N, Moretti C, Holtmaat A, Panzeri S, Fellin T (2020) Temporal sharpening of sensory responses by layer V in the mouse primary somatosensory cortex. Curr Biol 30:1589-1599.e10.
Vidoni ED, Acerra NE, Dao E, Meehan SK, Boyd LA (2010) Role of the primary somatosensory cortex in motor learning: An rTMS study. Neurobiol Learn Mem 93:532-539.
Viskontas IV, Ekstrom AD, Wilson CL, Fried I (2007) Characterizing interneuron and pyramidal cells in the human medial temporal lobe in vivo using extracellular recordings. Hippocampus 17:49-57.
Wang WW, Xie CL, Lu L, Zheng GQ (2014) A systematic review and meta-analysis of Baihui (GV20)-based scalp acupuncture in experimental ischemic stroke. Sci Rep 4:3981.
Wu P, Mills E, Moher D, Seely D (2010) Acupuncture in poststroke rehabilitation: a systematic review and meta-analysis of randomized trials. Stroke 41:e171-179.
Xing Y, Zhang M, Li WB, Dong F, Zhang F (2018) Mechanisms involved in the neuroprotection of electroacupuncture therapy for ischemic stroke. Front Neurosci 12:929.
Yao J, Zhang Q, Liao X, Li Q, Liang S, Li X, Zhang Y, Li X, Wang H, Qin H, Wang M, Li J, Zhang J, He W, Zhang W, Li T, Xu F, Gong H, Jia H, Xu X, Yan J, Chen X (2018a) A corticopontine circuit for initiation of urination. Nat Neurosci 21:1541-1550.
Yao LL, Grand T, Hanson J, Paoletti P, Zhou Q (2018b) Higher ambient synaptic glutamate at inhibitory versus excitatory neurons differentially impacts NMDA receptor activity. Nat Commun 9:4000.
Yao SQ, Liu Y, Cui S, Li HZ, Ji C, Yuan S, Ye QP, Zhang Y, Xu NG (2020) Effect of different frequencies of electroacupuncture on post-stroke dysphagia in mice. J Mol Neurosci 70:1871-1879.
Zhu HY, Lin WD, Zhao YX, Wang ZY, Lao WW, Kuang P, Zhou HG (2017) Transient upregulation of Nav1.6 expression in the genu of corpus callosum following middle cerebral artery occlusion in the rats. Brain Res Bull 132:20-27.

C-Editor: Zhao M; S-Editor: Li CH; L-Editors: Wetzel M, Li CH, Song LP; T-Editor: Jia Y

Additional Figures

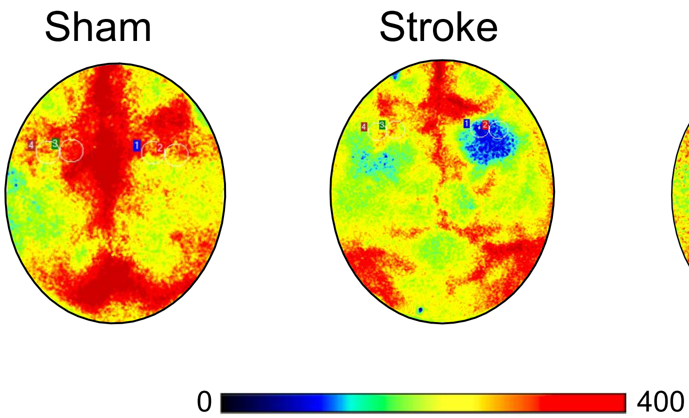

Additional Figure 1 Laser speckle blood flow imaging showed blood perfusion in the entire brain was decreased after stroke, while rescued by EA.

Sample images showing the blood perfusion in the sham (left), stroke (middle), and stroke + EA groups (right). It shows the low level of blood perfusion in the ipsilateral M1 after unilateral ischemia (blue indicates low blood perfusion). The blood perfusion recovery after EA treatment was represented. EA: Electroacupuncture; M1: primary motor cortex; S1: primary somatosensory cortex.

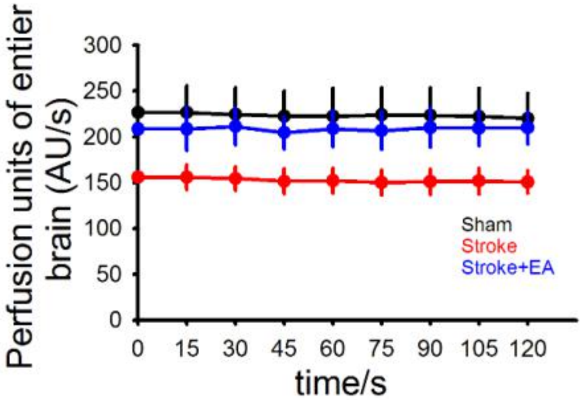

Additional Figure 2 The time course of perfusion blood in the entire brain in mice.

The blood perfusion of entire brain after stroke was rescued by electroacupuncture (EA) treatment. Data are presented as the mean ± SEM. Number of mice = 5 in the sham, stroke, stroke + EA groups, respectively.

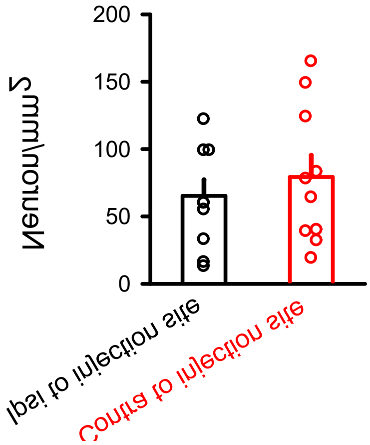

Additional Figure 3 Cell density of CTB488-positive neurons in the bilateral hemispheric S1 labeled by CTB tracer. Both S1 in the ipsilateral (black) and contralateral (red) to M1 CTB injection showed similar cell density of CTB488-positive neurons. There is no significance of CTB488-positive neurons between ipsilateral S1 and contralateral S1. The unpaired t-test was used for statistical analysis. Number of mice = 3. Number of slice =10. Contra: Contralateral; CTB488: Alexa Fluor retrograde cholera toxin B; EA: Electroacupuncture; Ipsi: Ipsilateral; M1: primary motor cortex; S1: primary somatosensory cortex.

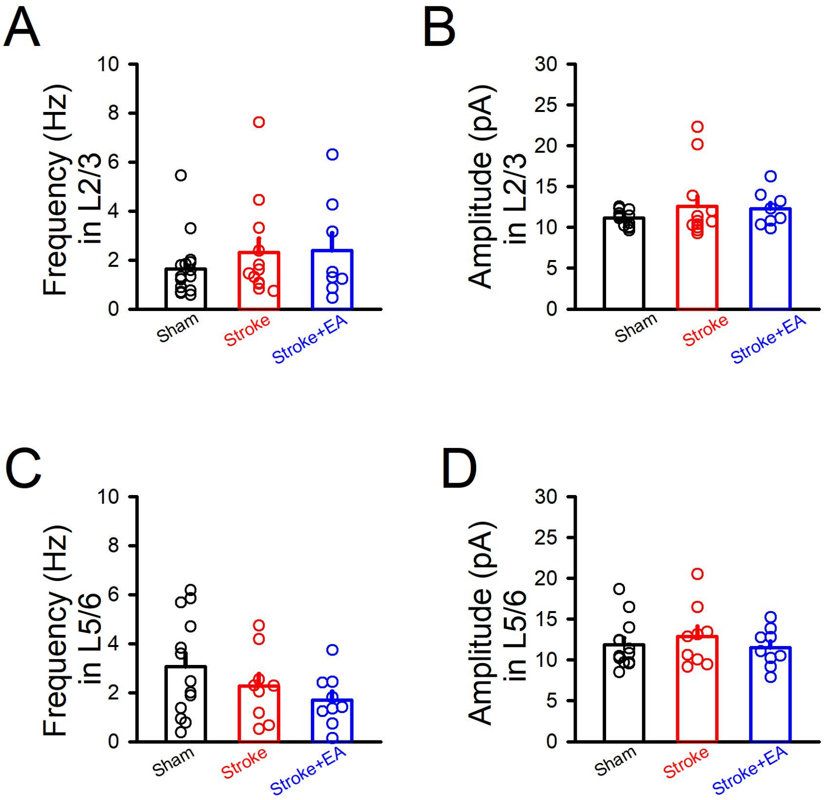

Additional Figure 4 The neuronal synaptic transmission in Layer 2/3 and Layer 5/6 located contralateral S1 is not altered after stroke or EA treatment.

The synaptic transmission in Layer 2/3 or Layer 5/6 located contralateral S1 is not altered in the stroke group or stroke+EA group, compared with the sham group. The frequency (A) or amplitude (B) of spontaneous excitatory post synaptic currents in Layer 2/3 or Layer 5/6 remained no change. Layer 2/3: Number of neurons =16, 12, 8 in the sham, stroke, and stroke + EA groups, respectively. Layer 5/6: Number of neurons = 13, 9, and 9 in the sham, stroke, and stroke + EA groups, respectively. Data are presented as the mean ± SEM. EA: Electroacupuncture; L2/3: Layer 2/3; L5/6: Layer 5/6; M1: primary motor cortex; S1: primary somatosensory cortex.

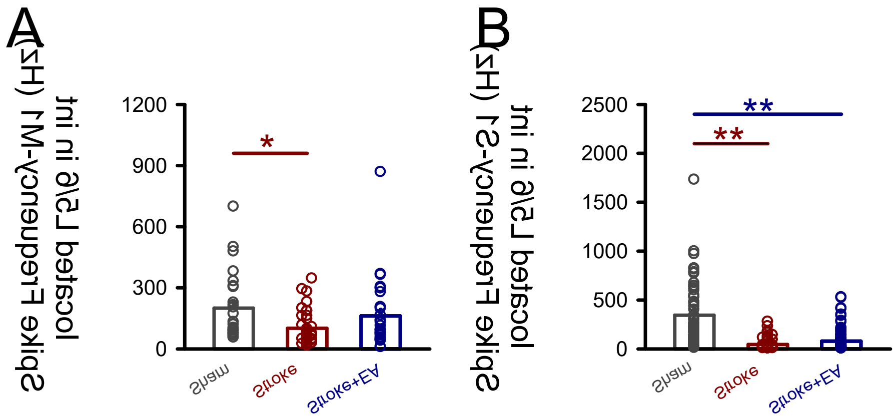

Additional Figure 5 The activity of inhibitory neurons in Layer 5/6 located contralateral M1 and S1 is decreased after stroke, while this impairment is not thoroughly rescued by EA treatment.

The inhibitory neuronal activity in Layer 5/6 located contralateral M1 and S1 is significantly impaired in Stroke group, and EA showed a tendency to enhance this impairment with no significance (A&B). Number of units in A = 25, 35, and 31 in the sham, stroke, and stroke + EA groups, respectively. Number of units in B =84, 60, and 103 in the sham, stroke, and stroke + EA groups, respectively. Data are presented as the mean ± SEM. *$P < 0.05$ (one-way analysis of variance with *post hoc* Bonferroni correction). EA: Electroacupuncture; Int: inhibitory neurons; L5/6: Layer 5/6; M1: primary motor cortex; S1: primary somatosensory cortex.

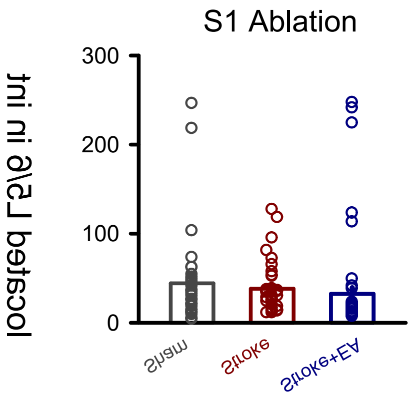

Additional Figure 6 The inhibitory neuronal activity *in vivo* in Layer 5/6 located contralateral M1 is not changed after stroke induction or EA treatment after S1 ablation.

The inhibitory neuronal activity in Layer 5/6 located contralateral M1 is no longer impaired in the stroke group after S1 ablation by taCasps virus infection, and EA showed no effect. Number of units = 33, 36, 57 in the sham, stroke, and stroke + EA groups, respectively. Data are presented as the mean ± SEM. EA: Electroacupuncture; Int: inhibitory neurons; L5/6: Layer 5/6; M1: primary motor cortex; S1: primary somatosensory cortex.